AIP | Applied Physics Letters

Control of tensile strain in germanium waveguides through silicon nitride layers

A. Ghrib, M. de Kersauson, M. El Kurdi, R. Jakomin, G. Beaudoin et al.

Citation: Appl. Phys. Lett. **100**, 201104 (2012); doi: 10.1063/1.4718525
View online: http://dx.doi.org/10.1063/1.4718525
View Table of Contents: http://apl.aip.org/resource/1/APPLAB/v100/i20
Published by the American Institute of Physics.

Control of tensile strain in germanium waveguides through silicon nitride layers

A. Ghrib,[1] M. de Kersauson,[1] M. El Kurdi,[1,a)] R. Jakomin,[2] G. Beaudoin,[2] S. Sauvage,[1] G. Fishman,[1] G. Ndong,[3] M. Chaigneau,[3] R. Ossikovski,[3] I. Sagnes,[2] and P. Boucaud[1,b)]
[1]*Institut d'Electronique Fondamentale, CNRS - Univ. Paris-Sud 11, Batiment 220, F-91405 Orsay, France*
[2]*Laboratoire de Photonique et de Nanostructures, CNRS - UPR 20, Route de Nozay 91460 Marcoussis, France*
[3]*Laboratoire de Physique des Interfaces et des Couches Minces, CNRS - Ecole polytechnique, F-91128 Palaiseau, France*

(Received 14 February 2012; accepted 1 May 2012; published online 15 May 2012)

Germanium ridge waveguides can be tensilely strained using silicon nitride thin films as stressors. We show that the strain transfer in germanium depends on the width of the waveguides. Carrier population in the zone center Γ valley can also be significantly increased when the ridges are oriented along the ⟨100⟩ direction. We demonstrate an uniaxial strain transfer up to 1% observed on the room temperature direct band gap photoluminescence of germanium. The results are supported by 30 band $\mathbf{k}\cdot\mathbf{p}$ modeling of the electronic structure and the finite element modeling of the strain field. © *2012 American Institute of Physics*. [http://dx.doi.org/10.1063/1.4718525]

A near-infrared germanium laser under optical pumping has been recently demonstrated.[1] One of the key ingredient to achieve lasing with this indirect band gap material is to decrease the energy separation between the L and zone center Γ valley and consequently to increase the population of the zone center conduction valley where the carriers recombine efficiently. This decreased energy separation can be obtained by applying a tensile strain to germanium. It has been shown that the larger the tensile strain, the lower the threshold to obtain optical gain.[2–6] Several strategies have thus been implemented to apply a tensile strain to germanium. The most direct strategy is to exploit the difference of thermal dilatation coefficients between germanium and silicon that can lead to a 0.25% tensile strain for germanium grown on silicon.[7] Growth on buffer layers with different lattice parameters like germanium-tin materials[8,9] or InGaAs buffer layers[10–12] is also a promising approach as it can lead to large tensile strain. The tensile strain can also be applied through mechanical stress on membranes of various thicknesses.[4,13–15] However, not all of these approaches are compatible with a laser integration on a silicon platform. The highly tensile strained layers might be too thin, tens of nm, as there is usually a trade-off between the magnitude of the strain and the thickness of the layer. The thickness of the germanium layer should be sufficiently large, hundreds of nm, for optical guiding and to meet the lasing condition with this material. The choice of the stressor is also important. Silicon nitride layers are particularly interesting as their deposition is fully compatible with complementary metal oxide semiconductor (CMOS) processing on a silicon platform. The use of nitride layers as stressors is now extensively used in the microelectronics industry. For photonics application, optical gain has been recently evidenced in germanium photonic wires strained by a Si_3N_4 layer indicating the potential of this approach.[16] Biaxial tensile strain larger than 1% has also been reported on germanium membranes with this method.[17] The effective strain present in the germanium layer is however strongly dependent on the Si_3N_4 deposition parameters, the geometry and the orientation of the layers, these parameters having a critical impact on the optical properties.[18]

In this Letter, we investigate the dependence of strain transfer from silicon nitride layers to germanium ridge waveguides. We show that the strain transfer significantly depends on the width of the waveguide, the strain being larger when the width of the waveguide is decreased. We also show that the orientation of the waveguide has a crucial importance. For a given uniaxial strain, the carrier population in the zone center Γ valley is significantly different between ⟨100⟩ and ⟨110⟩ orientations. These findings are supported by the modeling of the direct band gap room temperature photoluminescence of germanium waveguides studied under different configurations. Uniaxial strain up to 1% in germanium is experimentally demonstrated, with an enhanced carrier population at Brillouin zone center.

The investigated Ge films were grown on GaAs substrates by metal-organic chemical vapor deposition.[11,19] The nearly lattice-matched growth of Ge on GaAs makes possible to obtain high optical quality layers without dislocations. The germanium precursor is iso-butyl germane (IBGe) compatible with the III-V gas exhaust system. An AsH_3 flow is also supplied during Ge growth to realize highly *n*-doped layers. In these conditions, a free electron density of $8\times10^{18}\,cm^{-3}$ is measured at room temperature in germanium. The thickness of the deposited germanium film is 500 nm. The samples were first processed into ridge waveguides with various widths using inductively coupled plasma etching of germanium[20] followed by 1.2 μm vertical etching, i.e., no underetching, of GaAs. 600 and 450 nm thick nitride layers were then deposited on two different samples by plasma-enhanced chemical vapor deposition. The parameters for nitride deposition were varied in order to obtain different hydrostatic stress in the nitride layer. This translates into initial compressive hydrostatic stress values used in the modeling of 3 and 4.5 GPa for the 600 nm and 450 nm thick-nitride samples, respectively. The room temperature photoluminescence was

a)Electronic mail: moustafa.el-kurdi@u-psud.fr.
b)URL: http://pages.ief.u-psud.fr/QDgroup.

measured using a microphotoluminescence set-up coupled to a 50 cm grating spectrometer and an extended InGaAs photodetector.[21,22] The modeling of the photoluminescence spectra was based on a description of the band structure following a 30 band $\mathbf{k}\cdot\mathbf{p}$ formalism.[6,23,24] This formalism which accounts for the strain tensor calculated by finite elements provides a realistic description of the band structure all over the Brillouin zone on a multi-eV scale. The mixing between heavy hole and light hole bands is thus properly taken into account, and the dipole matrix elements can be calculated for any strain configurations. We did use as input parameters for the 30 band $\mathbf{k}\cdot\mathbf{p}$ formalism the values reported in Ref. 6, in particular −2.55 eV for $b_{\Gamma_5^+}$ and −9.75 eV for $a_{\Gamma_2^-}$. In Ref. 25, slightly different experimental values have been reported for these parameters. We have checked that these different sets of parameters lead within a meV to the same recombination energy for the luminescence involving the heavy hole band as the band gap energy scales at first order with the difference between $b_{\Gamma_5^+}$ and $a_{\Gamma_2^-}$. A band gap narrowing of 35 meV due to the doping of the layer was taken into account in agreement with Ref. 26. A 10 meV homogeneous linewidth at room temperature was considered for these highly doped materials. A photo-induced carrier density of $1\times10^{19}\,\mathrm{cm}^{-3}$ was taken into account. We did not include in the modeling the indirect band gap luminescence. As the ratio between direct and indirect band gap amplitudes can be dependent on non-radiative recombinations,[27] this would require to introduce in the modeling an adjustable parameter. Strain profiles as obtained from finite element modeling were considered for the calculations.

Fig. 1(a) shows a scanning electron microscope image of the ridge waveguides. One observes from bottom to top the etched GaAs layer, the tensile-strained Ge layer, and the Si_3N_4 stressor. The length of the waveguide is 50 μm as defined by lithography. Fig. 1(b) shows the calculated hydrostatic component $\varepsilon_{xx}+\varepsilon_{yy}+\varepsilon_{zz}$ of the strain profile for a 4 μm width waveguide. In this finite element modeling, the nitride layer is considered as hydrostatically strained, i.e., only diagonal elements are present in the stress tensor. The Young modulus for the nitride is 100 GPa. Only the nitride film on the top surface is considered as a stressor. The transferred strain is maximum at the top of the germanium layer. At the center of the Ge film in the x direction, the strain amplitude decreases regularly along the vertical z direction. The strain is rather homogeneous over the entire width of the germanium. In the following, the hydrostatic stress in the nitride layer was determined in order to obtain a good agreement for the emission of the narrowest waveguide. Once this parameter is fixed, the strain profile is calculated for each waveguide width without adjustable parameters. This strain profile is then used to calculate the radiative emission spectrum of the Ge film. This recombination spectrum is integrated over the inhomogeneously strained layer of germanium. In order to validate independently this procedure, micro-Raman measurements were performed on tensile-strained waveguides (not shown). The locally measured Raman peak shift can be converted into strain components under the assumption of uniaxial or biaxial plane stress. For the sample with 4 μm width and 3 GPa stress, the strain component ε_{xx} at the center of the waveguide is estimated at 0.62% by Raman and calculated at 0.7% by finite element. The average value of ε_{xx} deduced by Raman in a 2 μm window around the center is 0.69%.The agreement is thus very satisfying if we consider the assumptions for the Raman measurements.

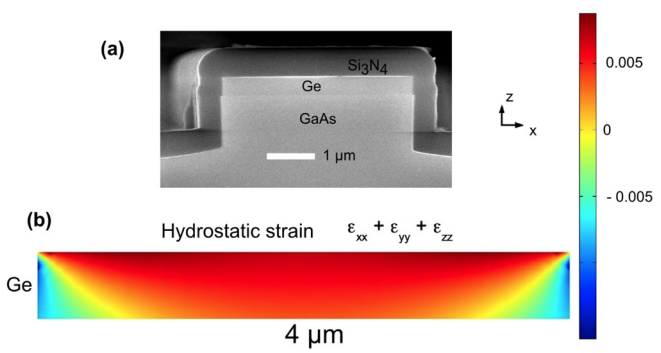

FIG. 1. (a) Scanning electron microscope image of the tensile-strained germanium waveguide. (b) Two-dimensional profile of the hydrostatic strain component in the germanium film. The width of the waveguide is 4 μm. The hydrostatic stress in the nitride film is 4.5 GPa. The right scale corresponds to the amplitude of the hydrostatic strain component.

Figure 2 shows the room temperature photoluminescence spectra of germanium ridges with several widths and for two distinct stress amplitudes in the nitride (3 GPa (Fig. 2(a)) and 4.5 GPa (Fig. 2(b)) equivalent hydrostatic stress). The ridges are oriented along ⟨100⟩ direction. The luminescence of these thin films is dominated by the direct band gap recombination. The modeling of the direct band gap photoluminescence is superimposed on the figures. We observe a very good agreement between the experimental photoluminescence spectra and the modeling of their high-energy line shape and energy maxima. As the width of the ridges is reduced, the photoluminescence maximum is red-shifted due to an increase of the tensile strain. This feature is a direct consequence of the pulling effect of the nitride in the direction perpendicular to the waveguide axis. For the 3 GPa

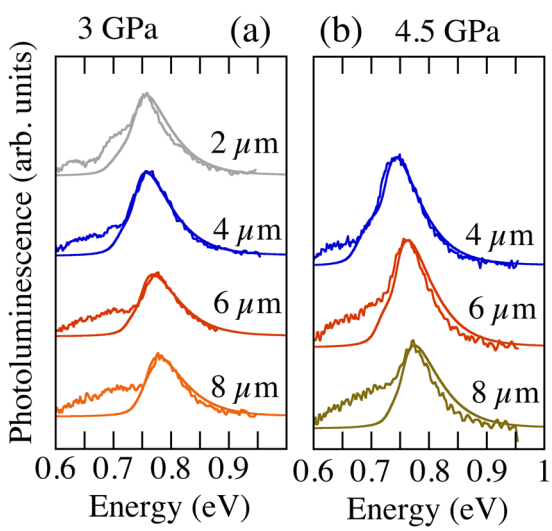

FIG. 2. (a) left: Room temperature photoluminescence spectra for variable waveguide widths. The smooth lines correspond to the modeling. The initial hydrostatic stress in the nitride film is 3 GPa. (b) Same as in (a), but for the 4.5 GPa nitride stressor. The curves have been offset for clarity. The difference in the thickness of the nitride layer contributes to the difference in amplitude. The indirect band gap recombination at low energy is not taken into account in the modeling.

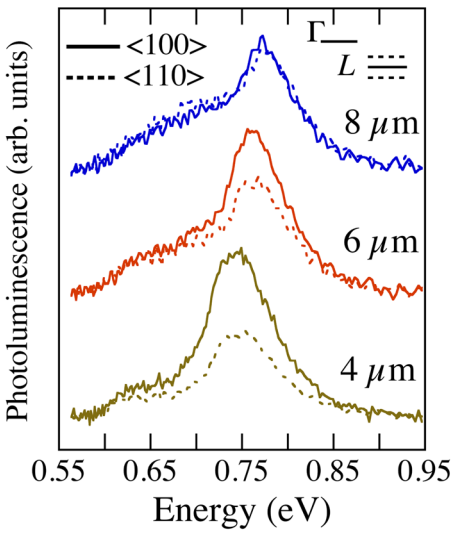

FIG. 3. Room temperature photoluminescence spectra for samples with variable widths and distinct orientations. The thick lines correspond to the ⟨100⟩ ridge direction. The dashed lines correspond to the ⟨110⟩ direction. The curves have been offset for clarity. The inset shows schematically the effect of the orientation on the energy splitting.

hydrostatic stress sample, the energy shift is around 50 meV corresponding to a strain parameter ε_{xx} from 0.33% (8 μm) to 0.87% (2 μm) at the top of the germanium layer. For the 4.5 GPa hydrostatic stress sample, the shift is even larger and an uniaxial strain of 1.07% is deduced for the 4 μm wide ridge. There is however a limit to the strain transfer. As the width of the waveguide is reduced, some plastic relaxation can occur: this has been observed for the 1 μm wide waveguide (3 GPa sample) and for widths equal or below 2 μm for the 4.5 GPa sample (not shown). This plastic relaxation is evidenced by cracks observed by optical microscopy. There is thus a trade-off between the ridge size and the effective strain that can be applied. The effect of reabsorption, not taken into account in the calculation, could explain the difference of broadening between experiment and modeling that is experimentally observed on some spectra. For the 2 μm width-3 GPa stress sample, the low-energy shoulder around 0.7 eV associated with the light-hole band is not perfectly reproduced by the modeling. An explanation of this feature is an enhanced redirection perpendicularly to the surface of the z-polarized photoluminescence (i.e., the components for the light-hole band) because of waveguide roughness. We emphasize that the applied uniaxial tensile strain of 1.07% for the 4 μm width-4.5 GPa stress sample has an equivalent effect on the band structure of germanium, i.e., a decrease of the Γ-L valley energy separation, as the one obtained with a biaxial tensile strain of half its value (0.53%). This effect is only obtained if the uniaxial strain is applied in the proper crystal direction as discussed below.

Figure 3 shows the comparison of the photoluminescence spectra for two distinct orientations of the ridge waveguides along ⟨100⟩ and ⟨110⟩ directions. The comparison is done for the 4.5 GPa sample, but similar results were obtained for the 3 GPa sample. As only the orientation of the ridge is modified, one can expect that all other parameters, like the non-radiative recombination and surface recombination, will remain constant. The difference of amplitude between both orientations can thus be quantitatively converted into a difference of carrier population in the zone center Γ valley. As seen, there is no amplitude difference for the 8 μm wide ridge. The difference becomes significant as the width of the ridge is reduced and is as large as a factor 2 for the 4 μm large waveguide. This feature indicates that the strain amplitude is not the only factor that governs the population of the zone center Γ valley. The orientation of the waveguide is of crucial importance if one wants to obtain high optical gain. This effect is a direct consequence of the difference between the strain tensors in the germanium. For the ⟨110⟩ direction, shear components appear in the stressor. These shear components do not modify significantly the recombination energy of the zone center conduction band. However, they lift the degeneracy in the L valley and consequently modify the carrier distribution in the L valley. We have computed the population ratio between Γ and L valley as a function of the uniaxial strain for two distinct orientations. The result is shown in Figure 4. Without strain, this ratio that accounts for the density of states of Γ and L valleys is equal to 1.6×10^{-4} at room temperature for a carrier population of $8 \times 10^{18}\,\mathrm{cm}^{-3}$ and a photo-induced carrier density of $1 \times 10^{19}\,\mathrm{cm}^{-3}$. As the uniaxial strain increases, the ratio increases for the ⟨110⟩ direction up to 1% uniaxial strain and decreases for higher values. This effect is due to the splitting of the L valley by the uniaxial strain and a subsequent energy lowering of this valley, which leads to an increased L-Γ energy separation. This situation is strikingly different for the ⟨100⟩ orientation as the ratio continuously increases as the strain increases. The photoluminescence amplitude difference between both orientations can be directly determined by the ratio of the data for a given strain. The inset of Fig. 4 shows the comparison between the ratio of photoluminescence amplitude between ⟨100⟩ and ⟨110⟩ orientations for both 4.5 GPa (as shown in Fig. 3) and 3 GPa stressed Si_3N_4 sample and the calculated ratio from the data in Fig. 4. A satisfying agreement is obtained with a population increase by a factor 2 for a 1% uniaxial strain. It indicates that laser devices processed following this approach should be preferentially oriented along ⟨100⟩ direction.

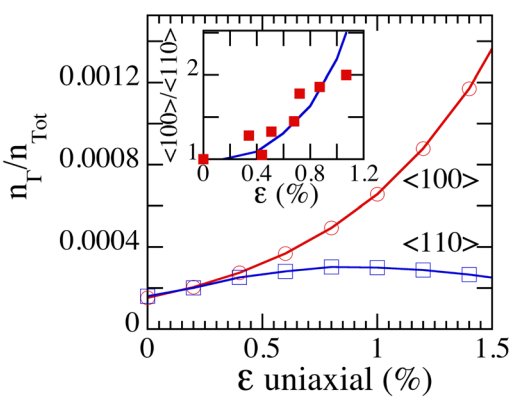

FIG. 4. Calculated room temperature ratio between the electron concentration in the Γ valley and the total electron concentration as a function of the uniaxial strain. The calculation is performed for two distinct orientations of the ridge. The inset shows the comparison between the predicted photoluminescence amplitude ratio between ⟨100⟩ and ⟨110⟩ orientations (full line) and the experimental data (squares).

In conclusion, we have shown that an efficient tensile strain transfer into germanium waveguide can be obtained using Si_3N_4 stressors. The strain transfer efficiency is dependent on the width of the waveguides. For a given waveguide width, the waveguide orientation also plays a critical role. Carrier population in the zone center Γ valley is significantly larger for waveguides oriented along ⟨100⟩ direction. These results should be considered for the design of germanium lasers using silicon nitride stressors in a process flow fully compatible with CMOS environment.

This work was supported by "Triangle de la Physique" under Gerlas convention and by Agence Nationale de la Recherche under GRAAL convention (ANR Blanc call 2011 BS03 004 01).

[1]J. Liu, X. Sun, R. Camacho-Aguilera, L. C. Kimerling, and J. Michel, Opt. Lett. **35**, 679 (2010).
[2]J. Liu, X. Sun, D. Pan, X. Wang, L. C. Kimerling, T. L. Koch, and J. Michel, Opt. Express **15**, 11272 (2007).
[3]S.-W. Chang and S. L. Chuang, IEEE J. Quantum Electron. **43**, 249 (2007).
[4]P. H. Lim, S. Park, Y. Ishikawa, and K. Wada, Opt. Express **17**, 16358 (2009).
[5]G. Pizzi, M. Virgilio, and G. Grosso, Nanotechnology **21**, 055202 (2010).
[6]M. El Kurdi, G. Fishman, S. Sauvage, and P. Boucaud, J. Appl. Phys. **107**, 013710 (2010).
[7]Y. Ishikawa, K. Wada, D. D. Cannon, J. Liu, H.-C. Luan, and L. C. Kimerling, Appl. Phys. Lett. **82**, 2044 (2003).
[8]J. Menendez and J. Kouvetakis, Appl. Phys. Lett. **85**, 1175 (2004).
[9]Y.-Y. Fang, J. Tolle, R. Roucka, A. V. G. Chizmeshya, J. Kouvetakis, V. R. D'Costa, and J. Menendez, Appl. Phys. Lett. **90**, 061915 (2007).
[10]Y. Bai, K. E. Lee, C. Cheng, M. L. Lee, and E. A. Fitzgerald, J. Appl. Phys. **104**, 084518 (2008).
[11]R. Jakomin, M. de Kersauson, M. El Kurdi, L. Largeau, O. Mauguin, G. Beaudoin, S. Sauvage, R. Ossikovski, G. Ndong, M. Chaigneau, I. Sagnes, and P. Boucaud, Appl. Phys. Lett. **98**, 091901 (2011).
[12]Y. Huo, H. Lin, R. Chen, M. Makarova, Y. Rong, M. Li, T. I. Kamins, J. Vuckovic, and J. S. Harris, Appl. Phys. Lett. **98**, 011111 (2011).
[13]M. El Kurdi, H. Bertin, E. Martincic, M. de Kersauson, G. Fishman, S. Sauvage, A. Bosseboeuf, and P. Boucaud, Appl. Phys. Lett. **96**, 041909 (2010).
[14]T.-H. Cheng, K.-L. Peng, C.-Y. Ko, C.-Y. Chen, H.-S. Lan, Y.-R. Wu, C. W. Liu, and H.-H. Tseng, Appl. Phys. Lett. **96**, 211108 (2010).
[15]J. R. Sanchez-Perez, C. Boztug, F. Chen, F. F. Sudradjat, D. M. Paskiewicz, R. Jacobson, M. G. Lagally, and R. Paiella, Proc. Natl. Acad. Sci. **108**, 18893 (2011).
[16]M. de Kersauson, M. El Kurdi, S. David, X. Checoury, G. Fishman, S. Sauvage, R. Jakomin, G. Beaudoin, I. Sagnes, and P. Boucaud, Opt. Express **19**, 17925 (2011).
[17]D. Nam, D. Sukhdeo, A. Roy, K. Balram, S.-L. Cheng, K. C.-Y. Huang, Z. Yuan, M. Brongersma, Y. Nishi, D. Miller, and K. Saraswat, Opt. Express **19**, 25866 (2011).
[18]F. Zhang, V. H. Crespi, and P. Zhang, Phys. Rev. Lett. **102**, 156401 (2009).
[19]M. de Kersauson, R. Jakomin, M. El Kurdi, G. Beaudoin, N. Zerounian, F. Aniel, S. Sauvage, I. Sagnes, and P. Boucaud, J. Appl. Phys. **108**, 023105 (2010).
[20]T.-P. Ngo, M. El Kurdi, X. Checoury, P. Boucaud, J. F. Damlencourt, O. Kermarrec, and D. Bensahel, Appl. Phys. Lett. **93**, 241112 (2008).
[21]V. Yam, V. Le Thanh, Y. Zheng, P. Boucaud, and D. Bouchier, Phys. Rev. B **63**, 033313 (2001).
[22]M. El Kurdi, T. Kociniewski, T.-P. Ngo, J. Boulmer, D. Debarre, P. Boucaud, J. F. Damlencourt, O. Kermarrec, and D. Bensahel, Appl. Phys. Lett. **94**, 191107 (2009).
[23]S. Richard, F. Aniel, and G. Fishman, Phys. Rev. B **70**, 235204 (2004).
[24]M. El Kurdi, S. Sauvage, G. Fishman, and P. Boucaud, Phys. Rev. B **73**, 195327 (2006).
[25]J. Liu, D. D. Cannon, K. Wada, Y. Ishikawa, D. T. Danielson, S. Jongthammanurak, J. Michel, and L. C. Kimerling, Phys. Rev. B **70**, 155309 (2004).
[26]S. Jain and D. Roulston, Solid-State Electron. **34**, 453 (1991).
[27]G. Grzybowski, R. Roucka, J. Mathews, L. Jiang, R. T. Beeler, J. Kouvetakis, and J. Menendez, Phys. Rev. B **84**, 205307 (2011).